# *tert*-Butylphosphonic Acid

## From the Bulk to the Gas Phase

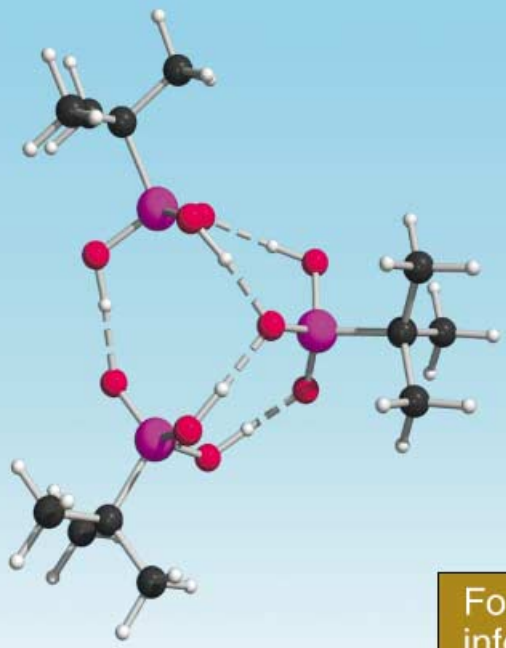

For more information read on...

X-RAY NMR ESI-MS DFT

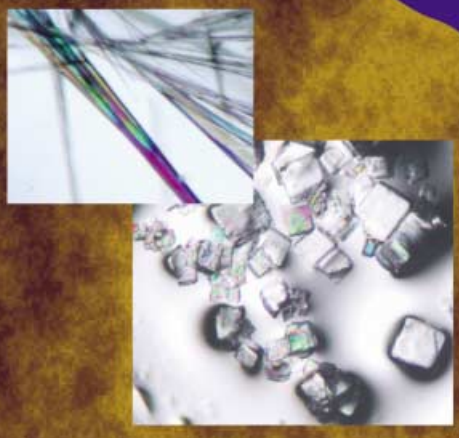

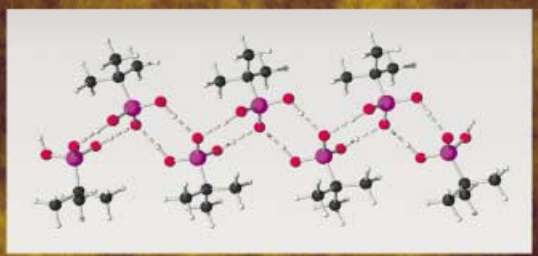

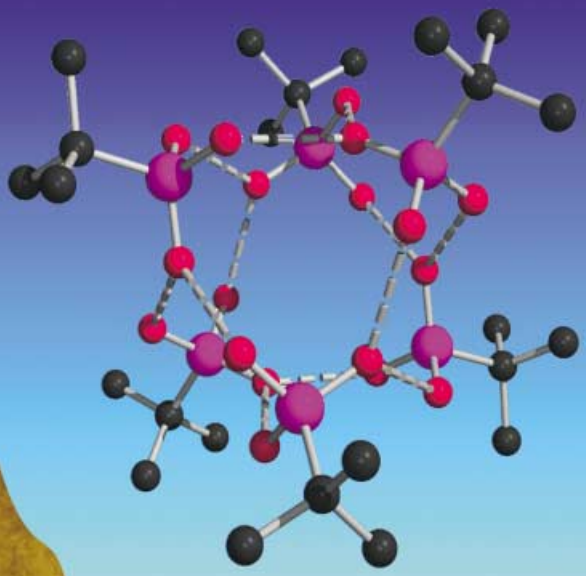

  0947-6539/03/0904-0837 $ 20.00+.50/0 

# *tert*-Butylphosphonic Acid: From the Bulk to the Gas Phase

**Michael Mehring,*[a] Markus Schürmann,[a] and Ralf Ludwig*[b]**

**Abstract**: The structure of *tert*-butylphosphonic acid in the solid, in solution, and in the gas phase was studied by single-crystal X-ray diffraction, $^{1}H$ and $^{31}P$ NMR spectroscopic studies in solution, solid-state $^{31}P$ NMR spectroscopy, and electrospray ionization mass spectrometry. In addition, density functional theory (DFT) calculations at the B3LYP/6-31G*, B3LYP/6-31 + G*, and B3LYP/6-311 + G* level of theory for a large number of H-bonded aggregates of the type $(t\mathrm{BuPO_3H_2})_n$ ($\mathbf{C}_n$, $\mathbf{P}_n$; $n = 1-7$) support the experimental work. Crystallization of $t\mathrm{BuPO_3H_2}$ from polar solvents such as $CH_3CN$ or THF gives the H-bonded one-dimensional polymer **2**, whereas crystallization from the less polar solvent $CDCl_3$ favors the formation of the H-bonded cluster $(t\mathrm{BuPO_3H_2})_6 \cdot CDCl_3$ (**1**). In $CDCl_3$ the hexamer $(t\mathrm{BuPO_3H_2})_6$ ($\mathbf{C_6}$) is replaced by smaller aggregates down to the monomer with decreasing concentration. DFT calculations and natural bond orbital (NBO) analyses for the clusters $\mathbf{C_1}-\mathbf{C_7}$ and the linear arrays $\mathbf{P_1}-\mathbf{P_7}$ reveal the hexamer $\mathbf{C_6}$ to be the energetically favored structure resulting from cooperative strengthening of the hydrogen bonds in the H-bonded framework. However, the average hydrogen bond strengths calculated for $\mathbf{C_6}$ and $\mathbf{P_2}$ do not differ significantly (42 – 43 kJ mol$^{-1}$). The average distances $r_{O\cdots O}$, $r_{O-H}$, $r_{P=O}$, and $r_{P-OH}$ in $\mathbf{C_1}-\mathbf{C_7}$ and $\mathbf{P_1}-\mathbf{P_7}$ are closely related to the hydrogen bond strength. Electrospray ionization mass spectrometry shows the presence of different anionic species of the type $[(t\mathrm{BuPO_3H_2})_n\text{-H}]^-$ ($\mathbf{A_1}-\mathbf{A_7}$, $n = 1-7$) depending on the instrumental conditions. DFT calculations at the B3LYP/6-31G* level of theory were carried out for $\mathbf{A_1}-\mathbf{A_6}$. We suggest the dimer $[(t\mathrm{BuPO_3H_2})_2\text{-H}]^-$ ($\mathbf{A_2}$) and the trimer $[(t\mathrm{BuPO_3H_2})_3\text{-H}]^-$ ($\mathbf{A_3}$) are the energetically favored anionic structures. A hydrogen bond energy of approximately 83 kJ mol$^{-1}$ was calculated for $\mathbf{A_2}$. Electrospray ionization mass spectrometry is not suitable to study the assembling process of neutral H-bonded *tert*-butylphosphonic acid since the removal of a proton from the neutral aggregates has a large influence on the hydrogen bond strength and the cluster structure.

**Keywords:** density functional calculations · hydrogen bonds · mass spectrometry · *tert*-butylphosphonic acid · X-ray diffraction

## Introduction

The continuing development of disciplines, such as supramolecular chemistry,[1] that exploit molecular recognition relies on a thorough understanding of the recognition properties of the functional groups involved in noncovalent interactions. The systematic analysis of inter- and intramolecular interactions by a large variety of experimental and computational methods has led to the expansion of our knowledge of noncovalent interactions, in particular of hydrogen bonding.[2, 3, 4] Although hydrogen bonds have been known for more than 100 years there is still a lively discussion about the fundamental aspects of the hydrogen bond itself and which type of interactions should be termed "hydrogen bond".[3, 5] Without doubt interactions of the type X–H ··· A, in which X is a proton donor and A is a proton acceptor, play a significant structure-directing role in all areas of chemistry ranging from biochemistry to materials science. These interactions span a large range of bond energies from weak interactions of approximately 1 kJ mol$^{-1}$ to strong interactions of up to 160 kJ mol$^{-1}$.[3] Phosphinic and phosphonic acids are considered to form strong hydrogen bonds and they can act simultaneously as proton donor and proton acceptor. As a result phosphinic acids usually dimerize[6] or form one-dimensional polymers,[7] and phosphonic acids typically crystallize in the form of polymeric associates.[8, 9, 10] Furthermore, the cocrystallization of phosphonic acids and amines gives access to a large variety of robust supramolecular assemblies based on strong hydrogen bonds.[4, 11, 12]

Herein, we present a combination of experimental and theoretical techniques to determine the structure of hydro-

[a] Dr. M. Mehring, Dr. M. Schürmann
Lehrstuhl für Anorganische Chemie II
Fachbereich Chemie der Universität Dortmund
Otto-Hahn-Strasse 6, 44221 Dortmund (Germany)
Fax: (+49) 231-755-5048
E-mail: mmeh@platon.chemie.uni-dortmund.de

[b] Priv.-Doz. Dr. R. Ludwig
Physikalische Chemie IIa
Fachbereich Chemie der Universität Dortmund
Otto-Hahn-Strasse 6, 44221 Dortmund (Germany)
Fax: (+49) 231-755-3937
E-mail: ludwig@pc2a.chemie.uni-dortmund.de

Supporting information for this article is available on the WWW under http://www.wiley-vch.de/home/chemeurj.org/ or from the author.

  0947-6539/03/0904-0838 $ 20.00+.50/0 

gen-bonded *tert*-butylphosphonic acid in the solid state, in solution, and in the gas phase. The array of experimental and theoretical methods employed comprises single-crystal X-ray diffraction, NMR spectroscopy, ESI/mass spectrometry, and quantum-mechanical calculations. The correlation of the above-mentioned methods leads to a description of a range of different structures present in all physical states including a polymeric and a cluster-type structure of solid *tert*-butylphosphonic acid.

## Results and Discussion

**X-ray single-crystal structure analysis of hexameric *t*BuPO$_3$H$_2$**: Somewhat unexpectedly *t*BuPO$_3$H$_2$ crystallizes from $CDCl_3$ in the form of a hydrogen-bonded cluster (**1**) comprising six molecules (Figure 1). The crystallographic

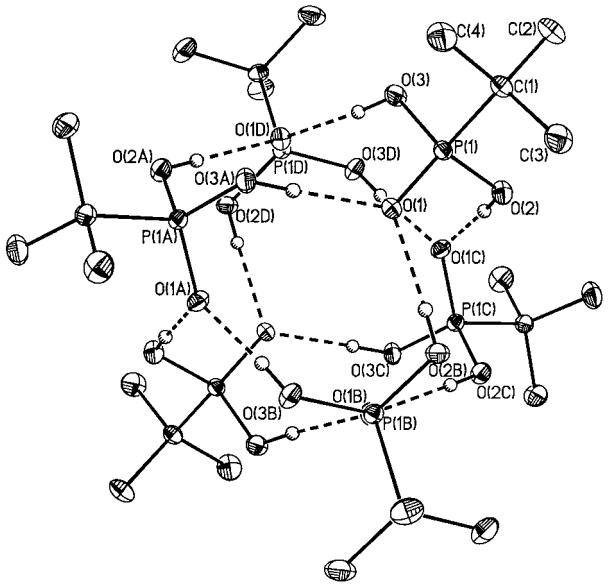


Figure 1. *tert*-Butylphosphonic acid: Hexameric cluster **1** as obtained by X-ray crystal structure analysis. General view (SHELXTL) showing 30% probability displacement ellipsoids and the atom-numbering scheme. Symmetry transformations: A: $x-y+1/3$, $x-1/3$, $-z-1/3$; B: $-y+1$, $x-y$, $z$; C: $-x+y+1$, $-x+1$, $z$; D: $y+1/3$, $-x+y+2/3$, $-z-1/3$.

data are given in Table 1 and selected bond lengths and angles are listed in Tables 2 and 3. The hexameric clusters are well separated from each other and $CDCl_3$ is found to fill the voids in the crystal lattice without showing any significant intermolecular interactions. In contrast, the solid-state structures of phosphonic acids reported so far are characterized by the formation of polymeric arrays of the acid as a result of strong intermolecular hydrogen bonds.[8, 9, 10] In cluster **1** all OH bonds are involved in hydrogen bonding, and a slightly distorted octahedron with the phosphorus atoms occupying the corners is formed. Each P=O oxygen atom participates in two hydrogen bonds, while each P–O(H) group forms a single hydrogen bond to a P=O oxygen atom.

The observed structure is in good agreement with the calculated hexameric cluster which was optimized by using the B3LYP/6-31G* level of theory. The measured intermo-

Table 1. Crystallographic data for compounds **1** and **2**.

| | **1** | **2** |
|---|---|---|
| empirical formula | $C_{4.33}H_{11.11}Cl_1O_3P_1$ | $C_4H_{11}O_3P$ |
| formula weight | 177.89 | 138.10 |
| crystal system | trigonal | monoclinic |
| space group | $R\bar{3}$ | $C2/c$ |
| $a$ [Å] | 16.3165(4) | 22.7291(6) |
| $b$ [Å] | 16.3165(4) | 6.3401(2) |
| $c$ [Å] | 16.7613(4) | 29.7196(10) |
| $\alpha$ [°] | 90 | 90 |
| $\beta$ [°] | 90 | 107.3796(11) |
| $\gamma$ [°] | 120 | 90 |
| volume [Å$^3$] | 3864.49(16) | 4087.2(2) |
| $Z$ | 18 | 24 |
| $\rho_{calcd}$ [Mg m$^{-3}$] | 1.376 | 1.347 |
| $\mu$ [mm$^{-1}$] | 0.579 | 0.329 |
| crystal size [mm$^3$] | $0.28\times0.25\times0.25$ | $0.40\times0.02\times0.02$ |
| $\theta$ range for data collection | 3.65 to 25.01 | 2.93 to 25.35 |
| reflections collected | 7236 | 27065 |
| independent reflections | 1449 [$R_{int}=0.024$] | 3673 [$R_{int}=0.039$] |
| data/restraints/parameters | 1449/0/96 | 3673/0/250 |
| goodness-of-fit on $F^2$ | 1.027 | 1.009 |
| $R$ indices [$I>2\sigma(I)$] | $R1=0.0357$ | $R1=0.0496$ |
| | $wR2=0.0720$ | $wR2=0.0874$ |
| $R$ indices (all data) | $R1=0.0518$ | $R1=0.1106$ |
| | $wR2=0.0777$ | $wR2=0.1021$ |
| largest diff. peak and hole [e Å$^{-3}$] | 0.506/−0.535 | 0.326/−0.392 |

Table 2. Selected bond lengths and angles for $(t\text{BuPO}_3\text{H}_2)_6\cdot CDCl_3$ (**1**) and $(t\text{BuPO}_3\text{H}_2)_n$ (**2**).[a]

| **1** | | **2** | |
|---|---|---|---|
| bond lengths [pm] | | | |
| P(1)–O(1) | 150.83(16) | P(1)–O(1) | 154.2(2) |
| P(1)–O(2) | 155.44(17) | P(1)–O(2) | 155.7(2) |
| P(1)–O(3) | 154.48(16) | P(1)–O(3) | 150.6(2) |
| O(1)–O(2B) | 259.6(2) | O(1)–O(3A) | 257.9(3) |
| O(1)–O(3A) | 254.1(2) | O(2)–O(3B) | 264.6(3) |
| O(2)–O(1C) | 259.6(2) | P(2)–O(13) | 150.9(2) |
| O(3)–O(1D) | 254.1(2) | P(2)–O(11) | 154.9(2) |
| | | P(2)–O(12) | 155.1(2) |
| | | O(11)–O(23C) | 260.2(3) |
| | | O(12)–O(23) | 264.6(3) |
| | | O(13)–O(22) | 262.3(3) |
| | | O(21)–O(13D) | 257.9(3) |
| | | P(3)–O(21) | 155.1(2) |
| | | P(3)–O(22) | 156.1(2) |
| | | P(3)–O(23) | 150.3(2) |
| angles [°] | | | |
| O(1)-P(1)-O(2) | 110.70(9) | O(1)-P(1)-O(2) | 105.14(15) |
| O(1)-P(1)-O(3) | 112.41(9) | O(1)-P(1)-O(3) | 112.23(12) |
| O(2)-P(1)-O(3) | 110.29(10) | O(2)-P(1)-O(3) | 110.29(10) |
| O(1)-P(1)-C(1) | 112.31(10) | O(1)-P(1)-C(1) | 105.57(14) |
| O(2)-P(1)-C(1) | 105.74(10) | O(2)-P(1)-C(1) | 108.35(14) |
| O(3)-P(1)-C(1) | 105.05(10) | O(3)-P(1)-C(1) | 112.02(14) |
| P(1)-O(1)-O(3A) | 123.66(9) | P(1)-O(1)-O(3A) | 118.62(13) |
| P(1)-O(1)-O(2B) | 122.53(9) | P(1)-O(2)-O(3B) | 112.72(13) |
| O(3A)-O(1)-O(2B) | 113.69(8) | | |
| P(1)-O(2)-O(1C) | 112.69(9) | | |
| P(1)-O(3)-O(1D) | 121.80(10) | | |

[a] Symmetry transformations used to generate equivalent atoms. **1**: A: $x-y+1/3, x-1/3, -z-1/3$; B: $-y+1, x-y, z$; C: $-x+y+1, -x+1, z$; D: $y+1/3, -x+y+2/3, -z-1/3$; **2**: A: $-x+1/2, y-1/2, -z-1/2$; B: $-x+1/2, y+1/2, -z+1/2$; C: $x, y-1, z$; D: $x, y+1, z$.

  0947-6539/03/0904-0839 $ 20.00+.50/0 

Table 3. Hydrogen bond parameters for **1** and **2**.

| | O–H···O | O–H [pm] | H···O [pm] | O···O [pm] | O–H···O [°] |
|---|---|---|---|---|---|
| **1** | O(2)–H(2)···O(1C) | 77(3) | 183(3) | 259.6(2) | 177(3) |
| | O(3D)–H(3)···O(1C) | 82(3) | 172(3) | 254.1(2) | 175(3) |
| **2** | O(1)–H(1)···O(3A) | 73(3) | 185(3) | 257.9(3) | 176(4) |
| | O(2)–H(2)···O(3B) | 70(3) | 195(3) | 264.6(3) | 176(4) |
| | O(11)–H(11)···O(23C) | 74(3) | 187(3) | 260.2(3) | 173(3) |
| | O(12)–H(12)···O(23) | 80(3) | 185(3) | 264.6(3) | 179(4) |
| | O(21)–H(21)···O(13D) | 79(3) | 178(3) | 257.9(3) | 177(4) |
| | O(22)–H(22)···O(13) | 82(3) | 180(3) | 262.3(3) | 174(4) |

lecular O···O bond lengths and O–H···O angles that characterize the H-bond strength are found to be 254.1(2)/259.6(2) pm and 175(3)/177(3)°, respectively (Table 3). These values are consistent with the corresponding calculated values of 261.5–262.2 pm and 174.3–179.2° (see Table 4, $\mathbf{C_6}$). The structure conformation is based on the P–O···O angles of 112.69(9)°, 121.80(19)°, 122.53(9)°, and 123.66(9)°. The corresponding calculated values are found in the range 113.0–125.5°. A characteristic feature of **1** is the formation of two 12-membered $(O{=}P\text{-}O\text{-}H)_3$ rings (Scheme 1, **A**; e.g. P(1), P(1B) and P(1C) in Figure 1) in which each O=P-O-H moiety is bicoordinatively linked and participates in matched pairs of hydrogen bonds, once as a Lewis base (P=O···H) and once as a Lewis acid (O–H···O).

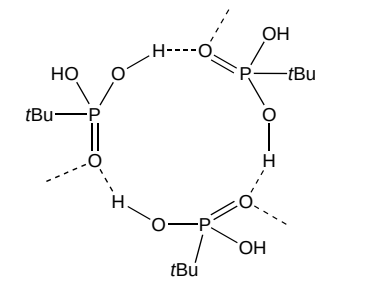


**A**

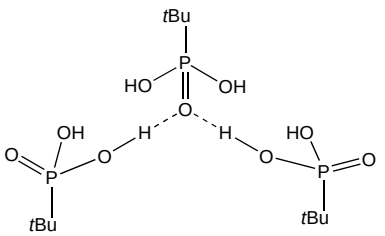


**B**

Scheme 1. Basic structural motifs in the cluster structure of $t\mathrm{BuPO_3H_2}$. Motif **A** shows the cooperative effect and motif **B** the anticooperative effect.

Such bicoordinate structures allow intermolecular electron delocalization (charge transfer) to occur in a maximally concerted manner, leading to strong non-pairwise additive enhancements of binding energies, referred to as the "cooperative effect".[2g, 13] Noteworthy, similar bonding situations are of general importance for phosphonic acids and are also present in the polymeric structures of acids such as $H_2O_3P(CH_2)_nPO_3H_2$ $(n = 1-4)$.[9, 12] In cluster **1** the two 12-membered $(O{=}P\text{-}O\text{-}H)_3$ rings of type **A** each contain three additional P–OH groups outside the ring which form hydrogen bonds to P=O groups of the second 12-membered ring. Thus, connectivity of type **B** is also observed in which the oxygen atom of the P=O group acts as a double acceptor for two hydrogen bonds. This "anticooperative effect" is expected to result in a weakening of hydrogen bonds.[13]

**DFT calculations of neutral clusters $\mathbf{C_1}$–$\mathbf{C_7}$**: To examine the factors that stabilize the hexameric hydrogen-bonded aggregate $(t\mathrm{BuPO_3H_2})_6$ we have carried out ab initio calculations on different cluster species from the monomer $\mathbf{C_1}$ to a heptamer $\mathbf{C_7}$ using the B3LYP/6-31G* level of theory (Figure 2). Recently, Wong efficiently calculated a large number of

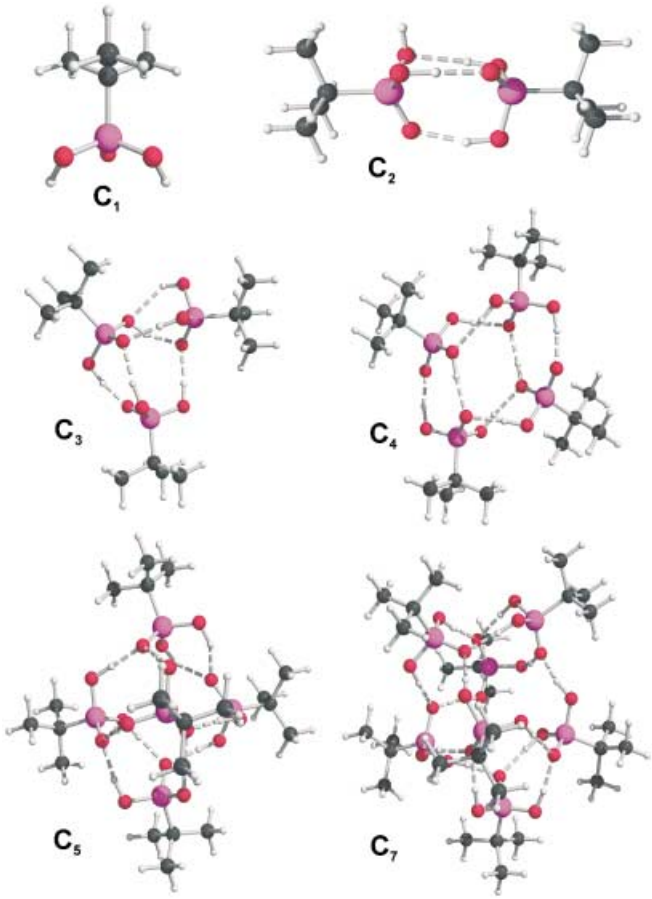


Figure 2. Optimized cluster geometry of $t\mathrm{BuPO_3H_2}$: $\mathbf{C_1}$–$\mathbf{C_5}$ and $\mathbf{C_7}$. Cluster $\mathbf{C_6}$ is omitted. The optimized geometry of $\mathbf{C_6}$ is similar to the molecular structure shown in Figure 1.

molecules including sulfur and phosphorus compounds using the B3LYP/6-31G* level of theory. The data sets gave strong support to hybrid density functionals compared with MP2 and the basis set used gave calculated frequencies that are in good agreement with measured values.[14] To compare the large clusters reported in this study, we were forced to use a uniform level of theory to get a reliable picture for all clusters. Thus we did not use larger basis sets but stuck to the well established



0947-6539/03/0904-0840 $ 20.00+.50/0 *Chem. Eur. J.* **2003**, *9*, No. 4

6-31G* basis set. However, to check the influence on the binding energy and geometry by including diffuse functions and by replacing the double zeta basis by a triple zeta basis, the monomer $\mathbf{C_1}$ (Figure 2) and the two dimers $\mathbf{C_2}$ and $\mathbf{P_2}$ (Figure 2, Figure 4) were optimized by using the 6-31 + G* and 6-311 + G* basis sets. Without giving all details[15] the results can be summarized as follows: There are slight changes observed for the distances of a selected bond but even for the largest deviations the difference between the calculated bond lengths using different basis sets do not exceed 1.5%. The average geometrical parameters do not differ significantly and no general trend is observed going from the smaller to the larger basis sets. The binding energies per molecule $\Delta E_{bin}$[16] were calculated for $\mathbf{C_2}$ to be 43.73, 40.77, and 42.99 kJ mol$^{-1}$ and for $\mathbf{P_2}$ to be 43.19, 42.98, and 45.47 kJ mol$^{-1}$ using the B3LYP/6-31G*, B3LYP/6-31 + G*, and B3LYP/6-311 + G* level of theory, respectively. The value calculated for the dimer $\mathbf{P_2}$ using the B3LYP/6-311 + G* level of theory is close to the value reported for the $Me_2P(O)OH$ dimer which is about 46 kJ mol$^{-1}$ per molecule calculated at the B3LYP/6-311 + G(3df,2p) level of theory on a B3LYP/6-31G* optimized geometry ignoring the basis set superposition error.[17] Our results show that the addition of diffuse functions and the use of the triple zeta basis does lead only to minor changes on the geometry and energies. Noteworthy, the use of the 6-31 + G* basis set gave slightly lower binding energies than those obtained with the 6-31G* basis set and the use of the 6-311 + G* basis set gave higher binding energies than those obtained with the 6-31 + G* basis set. However, the use of the B3LYP/6-311 + G* level of theory for all clusters is limited by computational restrictions. Consequently, the B3LYP/6-31G* level of theory was chosen to compare the hydrogen-bonded clusters of *tert*-butylphosphonic acid reported herein.

The optimized structures $\mathbf{C_1}$–$\mathbf{C_5}$ and $\mathbf{C_7}$ are shown in Figure 2; the optimized structure $\mathbf{C_6}$ is not given due to its similarity with the molecular structure of **1** (Figure 1). Selected geometrical data are given in Table 4. The formation of intermolecular hydrogen bonds results in increasing O–H and P=O and decreasing P–O(H) distances in the clusters $\mathbf{C_2}$–$\mathbf{C_6}$ compared with the monomer $\mathbf{C_1}$. The longest average O–H and P=O distances are observed for $\mathbf{C_6}$ (av $r_{O-H}$ = 101.08 pm, av $r_{P=O}$ 153.56 pm). In addition, going from $\mathbf{C_2}$ to $\mathbf{C_6}$ the average O···O and P–O(H) distances decrease and then again increase going to $\mathbf{C_7}$. Most importantly, the O–H···O angles in $\mathbf{C_6}$ are close to the optimum of 180° (av $\alpha_{O-H\cdots O}$ 176.91°), whereas in the other clusters significantly smaller O–H···O angles are observed. Even in the case of relatively short O···O distances an unfavorable O–H···O angle prevents an effective charge transfer resulting in weak hydrogen bonds.

Similar results are obtained by a comparison of the calculated energies for $\mathbf{C_1}$–$\mathbf{C_7}$: The B3LYP/6-31G* energies ($E_{B3LYP}$), the counterpoise-corrected energies ($E_{CP}$), the binding energies per molecule ($\Delta E_{bin}$) and per hydrogen bond ($\Delta E^*_{bin}$), and the NBO delocalization energies per molecule ($\Delta E_{deloc}$(NBO)) and per hydrogen bond ($\Delta E^*_{deloc}$(NBO)) are given in Table 5. The average binding energy per molecule $\Delta E_{bin}$ increases significantly with increasing cluster size going from the dimer $\mathbf{C_2}$ ($\Delta E_{bin}$ = 43.73 kJ mol$^{-1}$) to the hexamer $\mathbf{C_6}$ ($\Delta E_{bin}$ = 84.02 kJ mol$^{-1}$), which is a result of cooperative enhancement of hydrogen binding energies. Noteworthy, the heptamer $\mathbf{C_7}$ is less stable than the hexamer $\mathbf{C_6}$. The cooperative enhancement is less favorable in $\mathbf{C_7}$, which we attribute to a less effective charge transfer as a result of unfavorable O–H···O angles (av $\alpha_{O-H\cdots O}$ $\mathbf{C_6}$ 176.91°; $\mathbf{C_7}$ 172.01°). Consequently, the average binding energy per hydrogen bond is lowered from $\Delta E^*_{bin}$ = 42.01 kJ mol$^{-1}$ for $\mathbf{C_6}$ to $\Delta E^*_{bin}$ = 39.08 kJ mol$^{-1}$ for $\mathbf{C_7}$.

Table 4. Selected distances and angles for $\mathbf{C_1}$–$\mathbf{C_7}$ calculated at the B3LYP/6–31G* level of theory.

| Geometry | $\mathbf{C_1}$ | $\mathbf{C_2}$ | $\mathbf{C_3}$ | $\mathbf{C_4}$ | $\mathbf{C_5}$ | $\mathbf{C_6}$ | $\mathbf{C_7}$ |
|---|---|---|---|---|---|---|---|
| $r_{O-H}$ [pm] | 97.22 | 102.16 | 97.78 | 100.80 | 100.65 | 101.08 | 101.13 |
| | 97.22 | 97.27 | 100.73 | 100.53 | 100.68 | 101.21 | 100.36 |
| | | 98.23 | 100.05 | 100.80 | 100.66 | 101.10 | 100.17 |
| | | 99.88 | 102.93 | 100.53 | 100.97 | 101.22 | 101.60 |
| | | | 99.56 | 101.49 | 100.82 | 101.22 | 100.56 |
| | | | 99.92 | 98.78 | 100.43 | 101.10 | 100.91 |
| | | | | 101.49 | 100.74 | 101.16 | 101.21 |
| | | | | 98.78 | 100.99 | 101.12 | 100.57 |
| | | | | | 99.27 | 101.15 | 100.49 |
| | | | | | 100.36 | 101.12 | 100.91 |
| | | | | | | 101.20 | 101.05 |
| | | | | | | 101.08 | 100.25 |
| | | | | | | | 100.39 |
| | | | | | | | 100.56 |
| av $r_{O-H}$ [pm] | 97.22 | 99.39 | 100.15 | 100.40 | 100.56 | 101.15 | 100.73 |
| $r_{O\cdots O}$ [pm] | | 269.98 | 265.71 | 269.39 | 264.41 | 262.17 | 261.48 |
| | | 259.65 | 268.66 | 266.17 | 264.40 | 261.50 | 263.80 |
| | | 292.92 | 255.53 | 269.38 | 265.60 | 261.79 | 272.54 |
| | | | 272.47 | 266.17 | 262.31 | 261.76 | 256.59 |
| | | | 269.74 | 256.31 | 263.63 | 261.78 | 265.75 |
| | | | 301.22 | 283.25 | 264.01 | 261.81 | 263.38 |
| | | | | 256.31 | 263.89 | 261.59 | 263.78 |
| | | | | 283.25 | 261.64 | 261.49 | 261.46 |
| | | | | | 261.53 | 261.59 | 263.40 |
| | | | | | 267.71 | 261.50 | 265.84 |
| | | | | | | 261.49 | 262.01 |
| | | | | | | 262.20 | 263.51 |
| | | | | | | | 265.56 |
| | | | | | | | 262.59 |
| av $r_{O\cdots O}$ [pm] | | 274.18 | 272.22 | 268.78 | 263.91 | 261.72 | 264.33 |
| $\alpha_{O-H\cdots O}$ [°] | | 161.53 | 170.36 | 174.82 | 176.46 | 175.95 | 165.38 |
| | | 164.55 | 152.18 | 165.84 | 175.36 | 179.17 | 170.94 |
| | | 163.10 | 169.32 | 174.82 | 179.32 | 176.12 | 173.56 |
| | | | 168.20 | 165.84 | 178.50 | 178.40 | 168.96 |
| | | | 172.39 | 169.71 | 177.37 | 178.43 | 177.50 |
| | | | 138.90 | 168.83 | 169.71 | 176.12 | 173.13 |
| | | | | 169.72 | 170.12 | 174.25 | 170.68 |
| | | | | 168.84 | 174.48 | 177.82 | 171.02 |
| | | | | | 151.33 | 174.46 | 177.90 |
| | | | | | 144.08 | 177.81 | 171.08 |
| | | | | | | 178.95 | 177.09 |
| | | | | | | 175.45 | 172.83 |
| | | | | | | | 166.71 |
| | | | | | | | 171.40 |
| av $\alpha_{O-H\cdots O}$ [°] | | 163.06 | 161.90 | 169.80 | 169.67 | 176.91 | 172.01 |
| av $r_{P-O(H)}$ [pm] | | 160.89 | 160.59 | 160.49 | 159.42 | 158.93 | 159.10 |
| av $r_{P=O}$ [pm] | | 150.89 | 152.32 | 151.92 | 153.12 | 153.56 | 153.20 |

**X-ray single-crystal structure analysis of polymeric *t*Bu-$PO_3H_2$**: Crystallization of *tert*-butylphosphonic acid from the more polar solvents THF or $CD_3CN$ results in the formation of the one-dimensional H-bonded polymer **2** (Figure 3). The solvent of crystallization strongly influences the assembling

Table 5. Calculated B3LYP/6–31G* energy ($E_{B3LYP}$) and counterpoise corrected B3LYP/6–31G* energy ($E_{CP}$) for $\mathbf{C_1}$–$\mathbf{C_7}$ and $\mathbf{P_1}$–$\mathbf{P_7}$: Binding energy per molecule ($\Delta E_{bin}$) and per hydrogen bond ($\Delta E^*_{bin}$),[16] NBO delocalization energies per molecule ($\Delta E_{deloc}$(NBO)) and per hydrogen bond ($\Delta E^*_{deloc}$(NBO)).

| | $E_{B3LYP}$ | $E_{CP}$ | $\Delta E_{bin}$ | $\Delta E_{deloc}$ (NBO) | $\Delta E^*_{bin}$ | $\Delta E^*_{deloc}$ (NBO) |
|---|---|---|---|---|---|---|
| | per cluster [hartrees] | | per molecule [kJ mol$^{-1}$] | | per H-bond [kJ mol$^{-1}$] | |
| $\mathbf{C_1}$ | – 726.1509386 | – | – | – | | |
| $\mathbf{C_2}$ | – 1452.3435015 | – 1452.335189 | 43.73 | 169.87 | 29.25 | 113.22 |
| $\mathbf{C_3}$ | – 2178.5439958 | – 2178.523877 | 62.19 | 238.40 | 31.10 | 119.20 |
| $\mathbf{C_4}$ | – 2904.7355549 | – 2904.705875 | 67.03 | 268.99 | 33.52 | 134.52 |
| $\mathbf{C_5}$ | – 3630.9406356 | – 3630.900509 | 76.57 | 278.95 | 38.29 | 139.50 |
| $\mathbf{C_6}$ | – 4357.1478472 | – 4357.097635 | 84.02 | 295.31 | 42.01 | 147.65 |
| $\mathbf{C_7}$ | – 5083.3244513 | – 5083.264931 | 78.15 | 278.28 | 39.08 | 139.12 |
| $\mathbf{P_1}$ | – 726.1509387 | – | – | – | | |
| $\mathbf{P_2}$ | – 1452.3426619 | – 1452.334774 | 43.19 | 173.55 | 43.19 | 173.55 |
| $\mathbf{P_3}$ | – 2178.5315816 | – 2178.515331 | 54.71 | 213.84 | 41.03 | 160.37 |
| $\mathbf{P_4}$ | – 2904.7201746 | – 2904.695458 | 60.19 | 233.22 | 40.13 | 155.48 |
| $\mathbf{P_5}$ | – 3630.9090154 | – 3630.875234 | 63.30 | 246.31 | 39.56 | 153.93 |
| $\mathbf{P_6}$ | – 4357.0971488 | – 4357.055819 | 65.57 | 255.64 | 39.34 | 153.39 |
| $\mathbf{P_7}$ | – 5083.2861258 | – 5083.234832 | 66.86 | 257.65 | 39.00 | 150.29 |

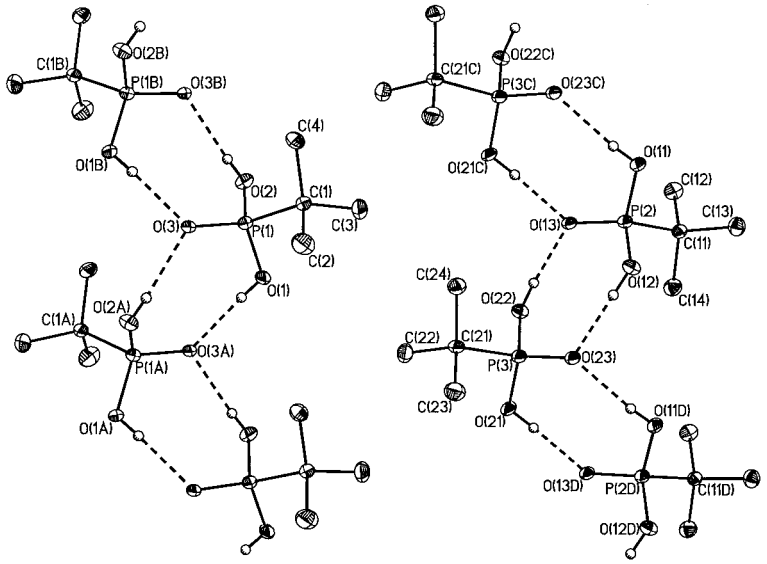


Figure 3. *tert*-Butylphosphonic acid: Polymeric **2** as obtained by X-ray crystal structure analysis. General view (SHELXTL) showing 30% probability displacement ellipsoids and the atom-numbering scheme. Two crystallographically independent chains of $t$BuPO$_3$H$_2$ are observed. Symmetry transformations: A: $-x+1/2$, $y-1/2$, $-z-1/2$; B: $-x+1/2$, $y+1/2$, $-z+1/2$; C: $x$, $y-1$, $z$; D: $x$, $y+1$, $z$.

process, and this has been thoroughly investigated previously.[18]

Two crystallographically independent $t$BuPO$_3$H$_2$ ribbons are formed as the result of crystal packing effects. Similar to **1** all OH bonds are involved in hydrogen bonding, each P–O(H) group forms a single hydrogen bond to a P=O oxygen atom and each of the P=O groups participates in two hydrogen bonds of different length (Scheme 2, **C**).

Pairs of shorter and longer hydrogen bonds are distinguished. The O···O distances are 257.9(3)/264.6(3) pm in one $t$BuPO$_3$H$_2$ ribbon, and 260.2(3)/264.6(3) and 257.9(3)/262.3(3) pm in the other one. Noteworthy, the average O···O distances in the two $t$BuPO$_3$H$_2$ ribbons are identical. Compared with the distances in the hexameric cluster **1** these are significantly longer in **2** (av $r_{O\cdots O}$: **1**, 256.9 pm; **2**, 261.3 pm), whereas the hydrogen bond angles O–H···O (range 173(3)° – 179(4)°) are comparable in both structures. Recently, the X-ray crystal structure analysis of a similar polymeric chain structure was reported for cyclohexylphosphonic acid (cy-Hex-PO$_3$H$_2$). However, in cy-Hex-PO$_3$H$_2$ symmetrical hydrogen bonds with O···O distances of 259.15(17) pm were observed.[10]

**DFT calculations of the oligomers $\mathbf{P_1}$–$\mathbf{P_7}$**: The general structural motif **C** as well as the distances and bond angles of the optimized oligomeric structures $\mathbf{P_2}$–$\mathbf{P_7}$ calculated at the B3LYP/6-31G*-level of theory are in reasonable agreement with the observed structure of **2**. Selected geometrical data are given in Table 6 and the optimized structure of $\mathbf{P_2}$ and $\mathbf{P_7}$ are shown in Figure 4 as representative examples. In addition, the B3LYP/6-31G* energies ($E_{B3LYP}$), the counter poise corrected energies ($E_{CP}$), the binding energies per molecule ($\Delta E_{bin}$) and per hydrogen bond ($\Delta E^*_{bin}$), and the NBO delocalization energies per molecule ($\Delta E_{deloc}$(NBO)) and per hydrogen bond ($\Delta E^*_{deloc}$(NBO)) for $\mathbf{P_1}$–$\mathbf{P_7}$ are given in Table 5.

In $\mathbf{P_1}$–$\mathbf{P_7}$ the average O–H distances increase from 97.2 pm to 100.2 pm, which results from a growing number of hydrogen bonds with favorable O–H···O angles. The average O–H···O angles range between 173.53 and 175.29° in $\mathbf{P_1}$–$\mathbf{P_7}$. Going from the dimer to the heptamer the number of hydrogen bonds per molecule increases from 1

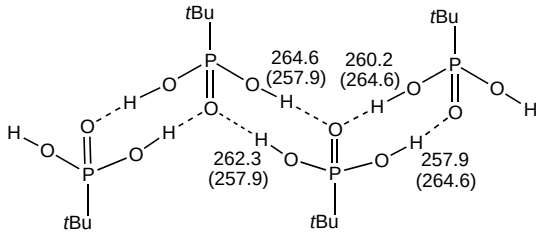


**C**

Scheme 2. Part of the polymeric chain structure of $t$BuPO$_3$H$_2$ (**2**). The O···O distances for the two crystallographically independent $t$BuPO$_3$H$_2$ ribbons are given in pm.



0947-6539/03/0904-0842 $ 20.00+.50/0 *Chem. Eur. J.* **2003**, *9*, No. 4

Table 6. Selected distances and angles for $\mathbf{P_1}-\mathbf{P_7}$ calculated at the B3LYP/6–31G* level of theory.

| Geometry | $\mathbf{P_1}$ | $\mathbf{P_2}$ | $\mathbf{P_3}$ | $\mathbf{P_4}$ | $\mathbf{P_5}$ | $\mathbf{P_6}$ | $\mathbf{P_7}$ |
|---|---|---|---|---|---|---|---|
| $r_{O-H}$ [pm] | 97.22 | 97.21 | 97.16 | 97.15 | 97.15 | 97.16 | 97.15 |
| | 97.22 | 101.14 | 100.93 | 100.78 | 100.76 | 100.78 | 100.71 |
| | | 101.14 | 101.73 | 101.29 | 101.28 | 101.45 | 101.29 |
| | | 97.21 | 100.76 | 100.38 | 100.26 | 100.35 | 100.22 |
| | | | 100.58 | 100.37 | 100.48 | 100.47 | 100.43 |
| | | | 97.20 | 101.28 | 100.82 | 100.86 | 100.68 |
| | | | | 100.77 | 100.70 | 100.86 | 100.74 |
| | | | | 97.15 | 100.94 | 100.47 | 100.31 |
| | | | | | 100.51 | 100.35 | 100.38 |
| | | | | | 97.20 | 101.45 | 100.82 |
| | | | | | | 100.77 | 100.62 |
| | | | | | | 97.16 | 100.93 |
| | | | | | | | 100.49 |
| | | | | | | | 97.20 |
| av $r_{O-H}$ [pm] | 97.22 | 99.18 | 99.73 | 99.90 | 100.01 | 100.18 | 100.15 |
| $r_{O\cdots O}$ [pm] | | 261.86 | 261.64 | 261.23 | 261.28 | 260.82 | 261.17 |
| | | 261.86 | 264.38 | 265.01 | 265.20 | 265.32 | 265.60 |
| | | | 263.38 | 265.97 | 265.77 | 265.82 | 267.06 |
| | | | 265.22 | 265.95 | 266.44 | 266.48 | 266.35 |
| | | | | 265.07 | 263.97 | 263.58 | 263.78 |
| | | | | 261.21 | 264.14 | 263.57 | 264.60 |
| | | | | | 265.56 | 266.48 | 266.39 |
| | | | | | 262.50 | 265.82 | 266.83 |
| | | | | | | 265.32 | 264.43 |
| | | | | | | 260.82 | 264.04 |
| | | | | | | | 265.82 |
| | | | | | | | 262.53 |
| av $r_{O\cdots O}$ [pm] | | 261.86 | 263.66 | 264.07 | 264.32 | 264.40 | 264.88 |
| $\alpha_{O-H\cdots O}$ [°] | | 175.29 | 172.65 | 170.29 | 169.80 | 169.12 | 169.72 |
| | | 175.29 | 175.91 | 174.41 | 174.29 | 174.06 | 174.20 |
| | | | 174.71 | 175.87 | 176.52 | 174.99 | 176.71 |
| | | | 176.56 | 175.83 | 176.15 | 176.84 | 176.17 |
| | | | | 170.35 | 172.49 | 171.91 | 171.37 |
| | | | | 174.43 | 171.97 | 171.90 | 171.36 |
| | | | | | 176.39 | 176.82 | 175.54 |
| | | | | | 174.47 | 174.98 | 177.41 |
| | | | | | | 174.07 | 172.31 |
| | | | | | | 169.12 | 171.86 |
| | | | | | | | 174.55 |
| | | | | | | | 177.13 |
| av $\alpha_{O-H\cdots O}$ [°] | | 175.29 | 174.96 | 173.53 | 174.01 | 173.38 | 174.03 |
| av $r_{P-O(H)}$ [pm] | 163.36 | 160.88 | 160.45 | 160.20 | 159.96 | 159.87 | 159.74 |
| av $r_{P=O}$ [pm] | 148.94 | 150.89 | 151.71 | 152.12 | 152.30 | 152.55 | 152.55 |

to 1.7, and consequently the average binding energy per molecule increases from $\Delta E_{bin} = 43.19\ kJ\,mol^{-1}$ for $\mathbf{P_2}$ to $\Delta E_{bin} = 66.86\ kJ\,mol^{-1}$ for $\mathbf{P_7}$. If only the O–H distances are considered which are involved in hydrogen bonding, the average O–H distance gradually decreases from 101.14 pm for $\mathbf{P_2}$ to 100.64 pm for $\mathbf{P_7}$ and the corresponding average O···O distances increase from 261.86 pm to 264.88 pm. In conclusion, we observe the strongest hydrogen bonds in the dimer $\mathbf{P_2}$. Adding an additional hydrogen bond to the dimer forces the phosphoryl oxygen atom to act as a double acceptor of type **B** ("anticooperative effect") which results in a weakening of the hydrogen bonds. This trend is reflected by the binding energy per hydrogen bond which decreases from $\Delta E^*_{bin} = 43.19\ kJ\,mol^{-1}$ to $\Delta E^*_{bin} = 39.00\ kJ\,mol^{-1}$ going from the dimer $\mathbf{P_2}$ to the heptamer $\mathbf{P_7}$. In contrast, the hydrogen bond energy per hydrogen bond in the cluster structures $\mathbf{C_2}$–$\mathbf{C_7}$, in which all OH groups are involved in hydrogen bonding, reaches a maximum for $\mathbf{C_6}$. Compared with $\mathbf{P_6}$ ($\Delta E^*_{bin} = 39.34\ kJ\,mol^{-1}$) the corresponding cluster $\mathbf{C_6}$ ($\Delta E^*_{bin} = 42.01\ kJ\,mol^{-1}$) is more stable as a result of 1) O–H···O angles close to 180° which allow an effective charge transfer and 2) the formation of the maximum number of hydrogen bonds.

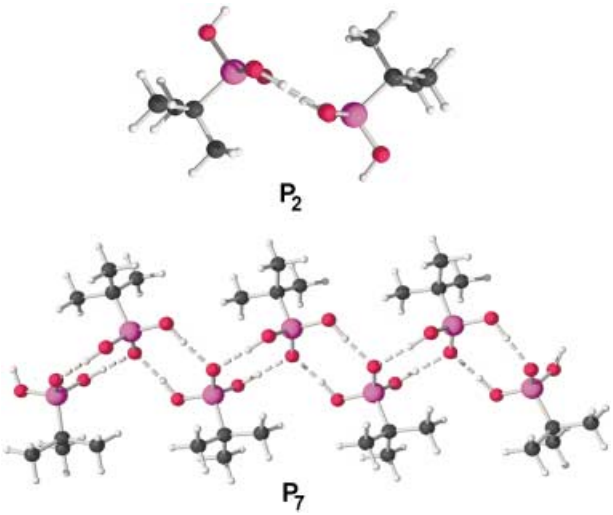


Figure 4. Optimized structures of the dimer $\mathbf{P_2}$ and the oligomer $\mathbf{P_7}$ calculated at the B3LYP/6–31G*-level of theory (carbon: black; oxygen: red; phosphorus: magenta).

**Natural bond orbital (NBO) analysis**: The NBO concept allows many of the quantitative trends in cluster structure, stability, and spectroscopic properties to be rationalized in terms of non-pairwise additive charge transfer delocalization between monomers. For example, the stabilization energy $\Delta E^{(2)} n_O \rightarrow \sigma^*_{OH}$ ($\Delta E_{deloc}$) is expected to be the principle attractive contribution to hydrogen bond formation. It is closely related to the cooperative strengthening and shortening of hydrogen bonds, since intermolecular charge delocalization enhances the Lewis base (donor) strength of one monomer and the Lewis acid (acceptor) strength of the other. The NBO delocalization energies per molecule ($\Delta E_{deloc}$) and per hydrogen bond ($\Delta E^*_{deloc}$) for $\mathbf{C_2}-\mathbf{C_7}$ and $\mathbf{P_2}-\mathbf{P_7}$ are listed in Table 5. For all clusters the stabilization energies per molecule $\Delta E_{deloc}$ are well correlated with the calculated cooperative binding energies $\Delta E_{bin}$. A plot of both energies versus each other gives a linear relationship (Figure 5).

The strongest intermolecular stabilization energy per molecule $\Delta E_{deloc} = 295.31\ kJ\,mol^{-1}$ is observed for $\mathbf{C_6}$, whereas the highest stabilization energy per hydrogen bond is observed for $\mathbf{P_2}$ with $\Delta E^*_{deloc} = 173.55\ kJ\,mol^{-1}$. In general, the stabilization energies are very large because it presents a pure attractive contribution, whereas the calculated binding energies also include steric repulsion of the filled orbitals $n_O$ and $\sigma^*_{OH}$. Noteworthy, the stabilization energy per hydrogen bond $\Delta E^*_{deloc}$ is larger in the oligomers $\mathbf{P_2}-\mathbf{P_7}$ than in the cluster $\mathbf{C_6}$. A favorable cluster geometry makes $\mathbf{C_6}$ the most stable species which is reflected by $\Delta E_{bin}$. In the series $\mathbf{P_2}-\mathbf{P_7}$ the attractive contribution $\Delta E^*_{deloc}$ of each additional hydrogen bond decreases but the stability of the aggregates ($\Delta E_{bin}$) increases by an increasing number of molecules. The decreas-

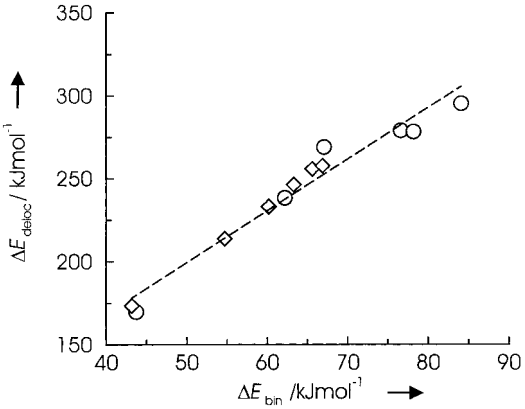


Figure 5. Correlation between the NBO delocalization energies per molecule ($\Delta E_{deloc}$) and the binding energies per molecule ($\Delta E_{bin}$) calculated for the neutral clusters $\mathbf{C}_2-\mathbf{C}_7$ (○) and the linear oligomers $\mathbf{P}_2-\mathbf{P}_7$ (◇).

ing values of $\Delta E^*_{deloc}$ are explained by the "anticooperative effect" which was discussed in the previous chapter.

The distances in the H-bonded fragments P=O···H–O–P show the expected trends with increasing hydrogen-bond strength indicated by larger binding energies. Increasing hydrogen-bond strength leads to lengthening of the P=O and O–H bonds, and shortening of the O–P and O···O distances, respectively. The binding energies $\Delta E_{bin}$ and the distances are correlated in a linear fashion (Figure 6). The opposing shift of the P–O relative to the O–H and P=O bond is rationalized in terms of a "charge transfer" or a "resonance" picture of hydrogen bonding.[19] Since the hydrogen bond is pictured as having significant "resonance hybrid" character ($O-H:O \leftrightarrow {}^{-}O:H-O^{+}$), it necessarily couples to other types of resonance delocalization, such as the resonance $O-P=O \leftrightarrow {}^{+}O=P-O^{-}$. Just as hydrogen bonding is known to be enhanced by resonance,[20] formation of hydrogen bonds strengthens the resonance in participating P–O groups by increasing the P–O double-bond character, while decreasing the P=O bond order. The pattern of the geometry shifts with cluster size is therefore fully consistent with this simple picture of coupled intramolecular/intermolecular resonance delocalization.

**Studies in solution:** The hexamer **1** is the most stable species in a saturated $CDCl_3$ solution. The $^1$H NMR chemical shift is concentration-dependent (Figure 7), and based on calculations of the $^1$H NMR chemical shifts it is correlated with the cluster size showing a downfield shift for larger clusters (Table 7, Figure 7).

In a saturated $CDCl_3$ solution of *tert*-butylphosphonic acid, hydroxyl proton chemical shifts of about $\delta = 10.40$ ppm relative to TMS are observed, which is in reasonable agreement with the calculated values of about $\delta = 9.61$ ppm for the hexameric cluster $\mathbf{C}_6$. The heptamer $\mathbf{C}_7$ gives a calculated chemical shift of $\delta = 9.17$ ppm, which indicates that the concentration of $\mathbf{C}_7$ is expected to be very low or even negligible. The calculated chemical shifts for the oligomers $\mathbf{P}_1-\mathbf{P}_7$ show a similar size-dependence but the values reach a plateau value of about $\delta = 8.0$ ppm, which is significantly lower than the experimental value. Thus the formation of linear arrays in $CDCl_3$ seems to be unlikely which in addition is supported by the fact that the formation of the maximum

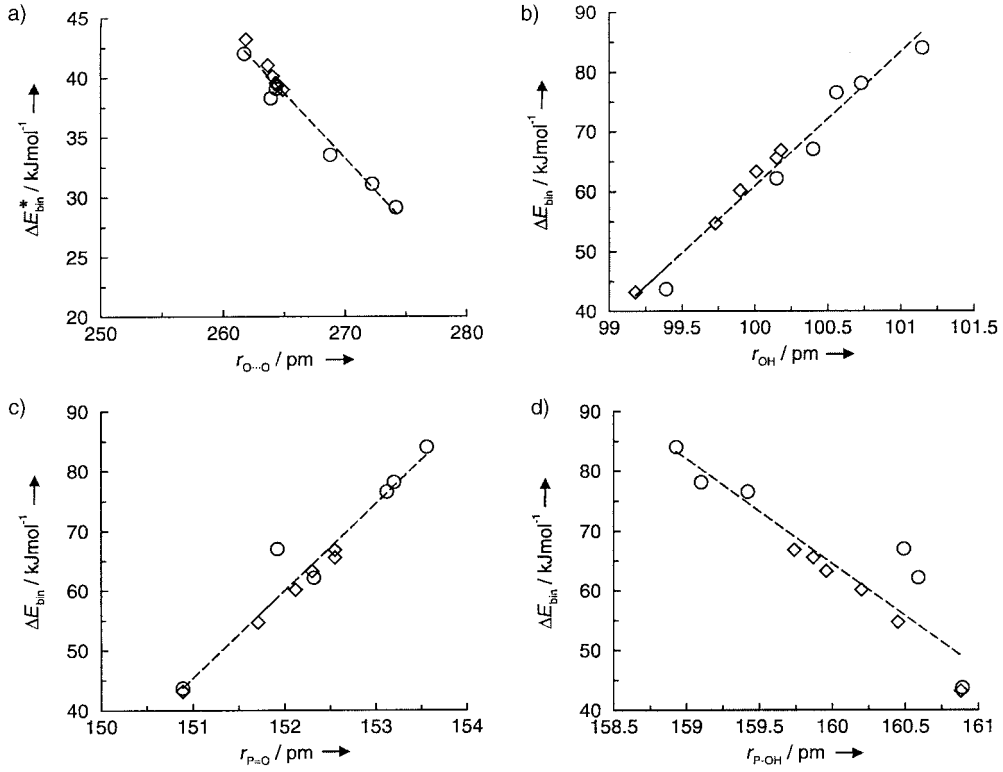


Figure 6. Correlation between a) the binding energy per hydrogen bond $\Delta E^*_{bin}$ and the intermolecular O···O distances, b) the binding energy per molecule $\Delta E_{bin}$ and the intramolecular O–H distances, c) $\Delta E_{bin}$ and the intramolecular P=O distances, and d) $\Delta E_{bin}$ and the intramolecular P–OH distances. Neutral clusters $\mathbf{C}_2-\mathbf{C}_7$ are represented by "○" and linear oligomers $\mathbf{P}_2-\mathbf{P}_7$ by "◇".



0947-6539/03/0904-0844 $ 20.00+.50/0 *Chem. Eur. J.* **2003**, *9*, No. 4

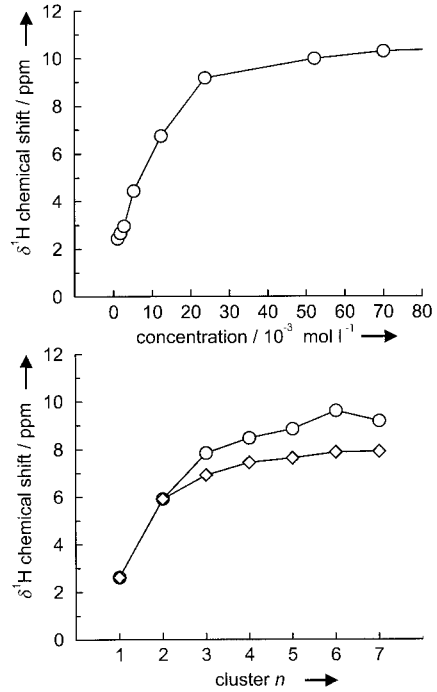


Figure 7. Experimental (top) and calculated (bottom) $^1$H NMR chemical shifts of $t$BuPO$_3$H$_2$; a) concentration dependence in CDCl$_3$; b) cluster size dependence of neutral clusters $\mathbf{C}_1-\mathbf{C}_7$ (○) and linear oligomers $\mathbf{P}_1-\mathbf{P}_7$ (◇).

Table 7. Calculated average isotropic hydroxyl proton and phosphorus chemical shielding values (ppm) for *tert*-butylphosphonic acid clusters $\mathbf{C}_n$ and linear oligomers $\mathbf{P}_n$ ($n=1-7$) at the B3LYP/6–31G* level. The chemical shift values were obtained by calculating and subtracting the values for corresponding references TMS and $H_3PO_4$.

| $\mathbf{C}_n$ | $^1$H | $^{31}$P | $\mathbf{P}_n$ | $^1$H | $^{31}$P |
|---|---|---|---|---|---|
| $\mathbf{C_1}$ | 2.62 | 41.28 | $\mathbf{P_1}$ | 2.62 | 41.28 |
| $\mathbf{C_2}$ | 5.91 | 45.47 | $\mathbf{P_2}$ | 5.91 | 41.28 |
| $\mathbf{C_3}$ | 7.84 | 47.06 | $\mathbf{P_3}$ | 6.93 | 42.87 |
| $\mathbf{C_4}$ | 8.46 | 41.87 | $\mathbf{P_4}$ | 7.44 | 43.94 |
| $\mathbf{C_5}$ | 8.84 | 41.71 | $\mathbf{P_5}$ | 7.63 | 43.70 |
| $\mathbf{C_6}$ | 9.61 | 40.19 | $\mathbf{P_6}$ | 7.88 | 44.95 |
| $\mathbf{C_7}$ | 9.18 | 41.31 | $\mathbf{P_7}$ | 7.91 | 44.47 |

number of hydrogen bonds is not possible. The H-bonded clusters $\mathbf{C}_2-\mathbf{C}_7$ are significantly lower in energy compared with the linear H-bonded chain structures $\mathbf{P}_2-\mathbf{P}_7$. Only the large number and high strength of the hydrogen bonds found in compounds such as **1** can lead to the observed strong downfield shift. Below a concentration of about $10^{-3}$ mol L$^{-1}$ the chemical shifts move upfield towards $\delta=2.44$ ppm, which is in good agreement with the calculated monomer value of about $\delta=2.62$ ppm.

Unfortunately the $^{31}$P NMR chemical shifts can not be used for cluster selection. The phosphorus atoms are not directly involved in hydrogen bonding and thus the predicted average $^{31}$P NMR chemical shifts for the linear arrays do not differ significantly from those of the clusters (Table 7). The measured chemical shifts of about $\delta=43$ ppm in CDCl$_3$, $\delta=40$ ppm in CD$_3$CN, and $\delta=43$ ppm in the solid state are in reasonable agreement with the calculated values for $\mathbf{C}_n$ and $\mathbf{P}_n$ in the range $\delta=40.2-47.1$ ppm. Overall we can conclude that in a saturated CDCl$_3$ solution the hexameric cluster is the dominant species but will be replaced by smaller clusters down to the monomer by decreasing concentration.

**ESI-MS studies of $t$BuPO$_3$H$_2$ and DFT calculations of anionic clusters of the type $[(t\mathrm{BuPO_3H_2})_n(t\mathrm{BuPO_3H})]^-$:** Recently, mass spectrometry[21] (ESI-MS,[22] FAB,[23] MALDI[24]) was shown to be a suitable analytical tool to study H-bonded structures that exhibit strong hydrogen bonds in the gas phase. In ESI-MS and MALDI experiments ion-labeling strategies were used to produce charged species to prevent destruction of the hydrogen-bonded network by protonation or deprotonation. These studies are restricted to compounds with appropriate ion-recognition properties. We wanted to test if ESI-MS measurements of hydrogen-bonded aggregates such as phosphonic acids provide useful structural information without the use of ion-labeling strategies. The reaction conditions in the ESI-MS experiment are usually very mild and it was shown for several examples that ESI-MS qualitatively reflected the charged species present in solution.[25] However, several factors such as instrumental conditions, solvent effects, analyte concentrations and gas-phase reactions might influence the appearance of ESI mass spectra.[26] In addition, to record ESI mass spectra of $t$BuPO$_3$H$_2$, proton transfer reactions must occur. To examine if there is a simple relationship between the neutral species in solution and the anionic species observed in the gas phase, the ESI-MS studies in the negative mode were supported by density functional (B3LYP) calculations for selected optimized anionic structures of the type $[(t\mathrm{BuPO_3H_2})_n(t\mathrm{BuPO_3H})]^-$ ($\mathbf{A_1}-\mathbf{A_6}$, Table 8, Figure 8). The input geometries for the anionic aggregates were obtained from the optimized geometries of $\mathbf{C_1}-\mathbf{C_6}$ by removal of an arbitrary chosen proton.

On condition that the detected anionic gas-phase species represents the most stable neutral aggregate, the hexamer $\mathbf{A_6}$ should dominate the ESI mass spectra. Instead a broad cluster population for $[(t\mathrm{BuPO_3H_2})_n-\mathrm{H}]^-$ with $n=1-7$ was observed at a desolvation gas temperature of 200 °C (Figure 9). Both increasing the temperature stepwise to 350 °C and increasing the cone skimmer voltage resulted in decreasing populations of larger clusters which is most likely a result of collusion induced fragmentation. At a desolvation gas temperature of 200 °C the population of the anionic trimer $\mathbf{A_3}$ was dominant, whereas at higher temperatures and at high cone voltages the signal of the highest intensity corresponds to the dimer $\mathbf{A_2}$ (Figure 9). The anionic cluster $\mathbf{A_6}$ was detected as a minor species only. Thus, the ESI-MS studies do not correlate well with our studies of $t$BuPO$_3$H$_2$ in solution. In addition, the density functional B3LYP calculations show that there is not a simple relationship between the neutral species in solution and the anionic aggregates in the gas phase. In general, the stabilization energies per molecule $\Delta E_{\mathrm{bin}}$ resulting from hydrogen bonding are significantly larger in the anionic clusters than in their neutral analogues (Table 9). Most importantly, the removal of a proton from the neutral species $\mathbf{C_1}-\mathbf{C_6}$ leads to different changes in energy per molecule depending on the cluster size. The energy difference per molecule between a neutral cluster and the corresponding anionic cluster becomes smaller as the cluster size increases

Table 8. Selected distances and angles for $\mathbf{A_1}-\mathbf{A_6}$ calculated at the B3LYP/6–31G* level of theory.

| Geometry | $\mathbf{A_1}$ | $\mathbf{A_{2a}}$ | $\mathbf{A_{2b}}$ | $\mathbf{A_3}$ | $\mathbf{A_4}$ | $\mathbf{A_5}$ | $\mathbf{A_6}$ |
|---|---|---|---|---|---|---|---|
| $r_{O-H}$ [pm] | 94.75 | 101.11 | 103.64 | 103.29 | 99.97 | 99.53 | 101.44 |
| | | 101.15 | 103.64 | 102.05 | 100.15 | 103.35 | 104.00 |
| | | 97.08 | 99.41 | 101.54 | 106.81 | 101.41 | 102.60 |
| | | | | 101.91 | 102.84 | 101.11 | 100.63 |
| | | | | 100.49 | 101.37 | 103.68 | 99.69 |
| | | | | | 100.90 | 101.82 | 102.80 |
| | | | | | 100.31 | 100.29 | 99.86 |
| | | | | | | 101.94 | 102.92 |
| | | | | | | 100.34 | 100.72 |
| | | | | | | | 100.81 |
| | | | | | | | 100.44 |
| av $r_{O-H}$ [pm] | 94.75 | 99.78 | | 101.86 | 101.76 | 101.50 | 101.45 |
| $r_{O\cdots O}$ [pm] | | 263.49 | 258.97 | 260.10 | 263.42 | 271.29 | 259.77 |
| | | 263.48 | 258.98 | 256.48 | 263.64 | 256.13 | 253.65 |
| | | | 278.89 | 260.63 | 262.12 | 260.35 | 255.01 |
| | | | | 259.94 | 248.64 | 261.56 | 264.75 |
| | | | | 266.32 | 257.61 | 257.71 | 267.53 |
| | | | | | 261.63 | 255.12 | 256.09 |
| | | | | | 266.76 | 263.18 | 268.20 |
| | | | | | | 265.00 | 255.81 |
| | | | | | | 258.40 | 263.64 |
| | | | | | | | 264.13 |
| | | | | | | | 264.73 |
| av $r_{O\cdots O}$ [pm] | | 263.49 | 265.61 | 260.69 | 260.55 | 260.97 | 261.21 |
| $\alpha_{O-H\cdots O}$ [°] | | 176.80 | 170.20 | 174.38 | 156.06 | 168.25 | 172.87 |
| | | 176.61 | 170.19 | 175.73 | 156.04 | 172.14 | 176.98 |
| | | | 163.59 | 175.50 | 173.91 | 173.18 | 175.91 |
| | | | | 172.71 | 176.56 | 169.75 | 170.02 |
| | | | | 173.79 | 176.15 | 171.48 | 174.27 |
| | | | | | 176.04 | 179.02 | 172.92 |
| | | | | | 175.52 | 170.82 | 169.39 |
| | | | | | | 176.89 | 172.77 |
| | | | | | | 175.78 | 178.10 |
| | | | | | | | 173.94 |
| av $\alpha_{O-H\cdots O}$ [°] | | 176.71 | 167.99 | 174.42 | 170.04 | 173.03 | 173.72 |
| av $r_{P-O(H)}$ [pm] | 165.42 | 162.64 | 161.41 | 160.08 | 159.74 | 159.55 | 159.79 |
| av $r_{P=O/P-O^-}$ [pm] | 148.21 | 151.49 | 152.62 | 152.60 | 152.50 | 152.58 | 152.37 |

and is 39.08 kJ mol$^{-1}$ for the dimers $\mathbf{C_2}$ and $\mathbf{A_{2b}}$ and 9.97 kJ mol$^{-1}$ for the hexameric aggregates $\mathbf{C_6}$ and $\mathbf{A_6}$. Thus different proton affinities are observed which depend on the cluster structure.

In the series $\mathbf{A_2}-\mathbf{A_6}$ the maximum stabilization energy of $\Delta E_{bin} = 97.36$ kJ mol$^{-1}$ per molecule is observed for the anionic aggregate $\mathbf{A_3}$, which is about 6.6 kJ mol$^{-1}$ per molecule higher than the $\Delta E_{bin}$ value of $\mathbf{A_6}$ ($\Delta E_{bin} = 90.78$ kJ mol$^{-1}$). In contrast to the neutral clusters $\mathbf{C_2}-\mathbf{C_7}$ and $\mathbf{P_2}-\mathbf{P_7}$ the calculated hydrogen bond energies per molecule $\Delta E_{bin}$ for $\mathbf{A_2}-\mathbf{A_6}$ do not increase with the cluster size. The high stability of the trimeric anion $\mathbf{A_3}$ results from the favorable geometry which allows a maximum delocalization of the negative charge to occur. Similar to $\mathbf{C_6}$ a twelve-membered $(O{=}P\text{-}O\text{-}H)_3$ ring (**A**) is formed "cooperative enhancement" and short O···O distances (av $r_{O\cdots O}$ 260.69 pm), long O–H bond lengths (av $r_{O-H}$ 101.86 pm) and favorable O–H···O bond angles (av 174.42°) characterize the cluster structure. Noteworthy, short O···O distances do not necessarily point at a very stable cluster topology. The shortest O···O distances were calculated for $\mathbf{A_4}$ but two unfavorable O–H···O bond angles of approximately 156° prevent an efficient charge transfer and thus make the structure less favorable than $\mathbf{A_3}$. A similar situation is

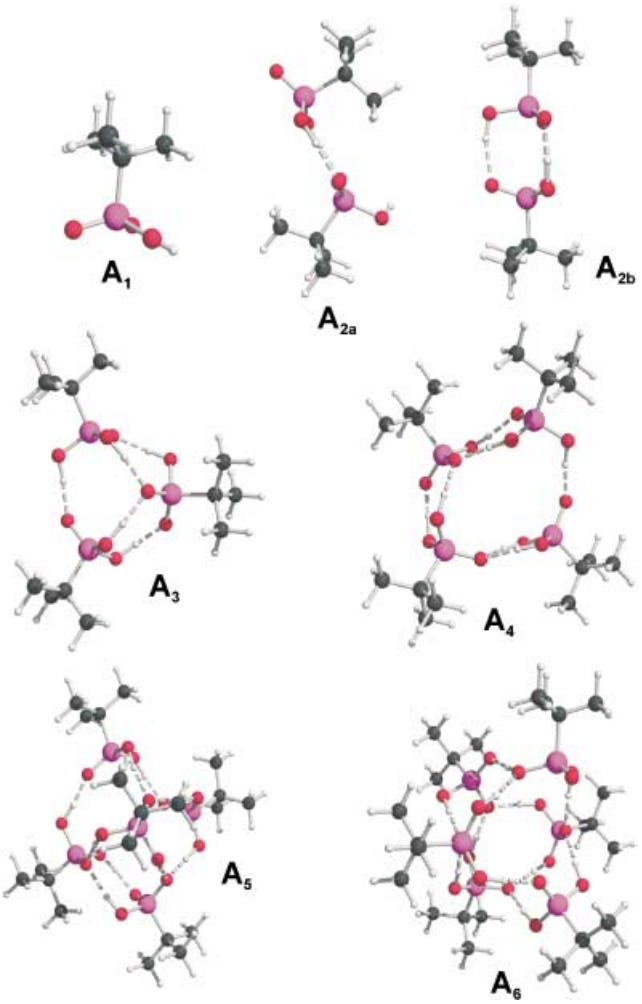


Figure 8. Optimized structures of the anionic clusters $\mathbf{A_1}-\mathbf{A_6}$ calculated at the B3LYP/6–31G* level of theory. Cluster $\mathbf{A_3}$ shows the highest average hydrogen bond energy per molecule for the anionic cluster series and in $\mathbf{A_{2a}}$ the strongest hydrogen bonds are observed (carbon: black; oxygen: red; phosphorus: magenta).

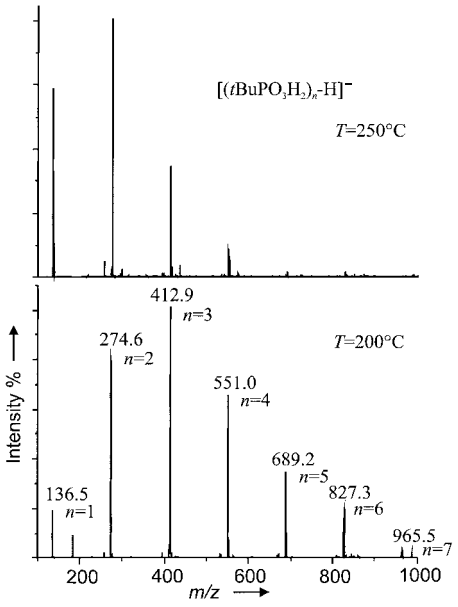


Figure 9. ESI mass spectra of $t$BuPO$_3$H$_2$ at desolvation gas temperatures of $T = 200$ and $T = 250$ °C.



0947-6539/03/0904-0846 $ 20.00+.50/0 *Chem. Eur. J.* **2003**, *9*, No. 4

Table 9. Calculated B3LYP/6–31G* energy ($E_{B3LYP}$) and counterpoise corrected B3LYP/6–31G* energy ($E_{CP}$) for the anionic clusters $\mathbf{A_1}$–$\mathbf{A_6}$: Binding energy per molecule ($\Delta E_{bin}$) and per hydrogen bond ($\Delta E^*_{bin}$), NBO delocalization energies per molecule ($\Delta E_{deloc}$(NBO)) and per hydrogen bond ($\Delta E^*_{deloc}$(NBO)).

| | $E_{B3LYP}$ | $E_{CP}$ | $\Delta E_{bin}$ | $\Delta E_{deloc}$ (NBO) | $\Delta E^*_{bin}$ | $\Delta E^*_{deloc}$ (NBO) |
|---|---|---|---|---|---|---|
| | per cluster [hartrees] | | per molecule [kJ mol$^{-1}$] | | per H-bond [kJ mol$^{-1}$] | |
| $\mathbf{A_1}$ | – 725.6009911 | – | – | – | – | – |
| $\mathbf{A_{2a}}$[a] | – 1451.827199 | – 1451.815037 | 82.81 | 269.74 | 82.81 | 269.74 |
| $\mathbf{A_{2b}}$[b] | – 1451.818764 | – 1451.807820 | 73.36 | 174.77 | 48.91 | 116.51 |
| $\mathbf{A_3}$ | – 2178.0369754 | – 2178.014159 | 97.36 | 320.45 | 58.42 | 192.27 |
| $\mathbf{A_4}$ | – 2904.2233062 | – 2904.193970 | 91.97 | 309.50 | 52.55 | 176.86 |
| $\mathbf{A_5}$ | – 3630.4271188 | – 3630.383738 | 93.99 | 293.55 | 52.22 | 163.08 |
| $\mathbf{A_6}$ | – 4356.6165011 | – 4356.563189 | 90.78 | 296.02 | 49.52 | 161.47 |

[a] Input geometry based on $\mathbf{P_2}$. [b] Input geometry based on $\mathbf{C_2}$.

observed for the two dimeric structures $\mathbf{A_{2a}}$ and $\mathbf{A_{2b}}$. Although $\mathbf{A_{2b}}$ forms two short hydrogen bonds ($r_{O\cdots O}$ 258.98 pm) and an additional longer hydrogen bond ($r_{O\cdots O}$ 278.89 pm) instead of two hydrogen bonds ($r_{O\cdots O}$ 263.49 pm) as observed for $\mathbf{A_{2a}}$, the latter is significantly lower in energy (Table 9). The difference is explained by the average hydrogen bond angles which are 176.71° for $\mathbf{A_{2a}}$ and 167.99° for $\mathbf{A_{2b}}$. The hydrogen bonds in the dimer $\mathbf{A_{2a}}$ are significantly stronger than those in the other structures. A hydrogen bond energy per hydrogen bond of 82.81 kJ mol$^{-1}$ provides a good explanation for the high intensity signals observed in the ESI-MS for the dimeric species.

## Conclusion

In this work we presented a combination of experimental and theoretical methods to determine the structure of the hydrogen-bonded *tert*-butylphosphonic acid in the solid, in solution, and in the gas phase. It allows a detailed analysis of species for all phases. A hexameric cluster ($\mathbf{C_6}$) is the dominant neutral species in solution and in the gas phase. In the H-bonded network of $\mathbf{C_6}$ all OH bonds are involved in hydrogen bonding and point towards the lone pairs of electrons on the phosphoryl oxygen atoms. By decreasing the concentration in the $CDCl_3$ solution the hexameric aggregate is replaced by smaller clusters down to the monomer. In the solid state both a one-dimensional hydrogen-bonded polymer and the hexameric cluster constitute two different structures which were obtained by a solvent-controlled assembling process. The use of the less polar $CDCl_3$ favors the formation of clusters to give a hydrophilic cluster core and a lipophilic cluster shell, whereas the formation of the polymer is observed from the more polar solvents $CH_3CN$ or THF.

Going to anionic clusters we suggest the trimer $[(t\mathrm{BuPO_3H_2})_2(t\mathrm{BuPO_3H})]^-$ ($\mathbf{A_3}$) and the dimer $[(t\mathrm{BuPO_3H_2})(t\mathrm{BuPO_3H})]^-$ ($\mathbf{A_{2a}}$) to be the favorite structures in the gas phase based on the combination of ESI-MS studies and DFT calculations. In the dimer $\mathbf{A_{2a}}$ strong hydrogen bonds were observed. A hydrogen bond energy of approximately 83 kJ mol$^{-1}$ was calculated at the B3LYP/6-31G* level of theory. In the neutral analogue $\mathbf{P_2}$ the hydrogen bond is significantly weaker and the hydrogen bond energy is approximately 43 kJ mol$^{-1}$.

Our results demonstrate that the combination of different geometrical parameters such as O···O and O–H distances along with the O–H···O angles provide information about favorable structure topologies in hydrogen-bonded clusters. The most stable species were observed for clusters which meet the following criteria: 1) a maximum number of hydrogen bonds, 2) short O···O distances, and 3) hydrogen bond angles close to 180°.

We have shown that the use of ESI-MS (negative mode) is not suitable for the structure analysis of neutral phosphonic acid cluster species in solution or even in the gas phase. To detect hydrogen-bonded clusters, the neutral species must be transformed to anionic clusters. The removal of a proton shows different effects on geometrical parameters and the binding energy for each cluster. Thus rearrangement processes in the gas phase most likely occur to give the most stable anionic aggregates.

We believe that our results will help to elucidate the assembling process of hydrogen-bonded phosphonic acid aggregates in all physical states and to develop rational design strategies for novel supramolecular arrays based on phosphonic acids and related hydrogen-bonded aggregates.

## Experimental Section

*tert*-Butylphosphonic acid was purchased from Aldrich and was dried in high-vacuum prior to use. Solvents were purified and dried by standard procedures.

$^1$H and $^{31}$P NMR spectra were recorded on a Bruker DRX 400 spectrometer operating at 400.13 and 161.98 MHz, respectively. Chemical shifts $\delta$ were referenced against $Me_4Si$ ($^1$H) and 85% $H_3PO_4$ ($^{31}$P). Electrospray ionization mass spectra were recorded in the negative mode on a Thermoquest–Finnigan instrument using $CH_3CN$ as the mobile phase. The compound was dissolved in $CH_3CN$ and than diluted with the mobile phase to give a solution of approximate concentration 0.1 mM. The sample was introduced by a syringe pump operating at 20 μL min$^{-1}$. The capillary voltage was 4.5 kV, while the cone-skimmer voltage was kept at – 70 V. The extraction cone voltage was – 20 V. The ion source temperature was varied between 200 and 350 °C. The $m/z$ values reported correspond to that of the most intense peaks in the corresponding isotope pattern.

Crystal data were collected on a Nonius Kappa CCD diffractometer. The structures were solved by direct methods (SHELXS97) and successive difference Fourier syntheses. Refinement applied full-matrix least-squares methods SHELX97. The hydrogen atoms of the OH groups were located in the difference Fourier map and refined isotropically.

CCDC-183675 (**1**) and CCDC-183676 (**2**) contain the supplementary crystallographic data for this paper. These data can be obtained free of charge via www.ccdc.cam.ac.uk/conts/retrieving.html (or from the Cambridge Crystallographic Center, 12 Union Road, Cambridge CB21EZ, UK; Fax: (+44) 1223-336033; or deposit@ccdc.cam.ac.uk).

## Computational Methods

Supramolecular calculations have been carried out at the density functional (B3LYP) level with the Gaussian 98 program[27] using the internal stored 6-31G*, 6-31+G*, and 6-311+G* basis sets. For the fully optimized hydrogen-bonded structures, the counterpoise-corrected binding energies[28] and the isotropic chemical shieldings have been calculated. Additionally, the wave functions were analyzed by the natural bond orbital (NBO) method,[29] a standard option of Gaussian 98. The NBO analysis explains the strength of hydrogen bonds in terms of donor–acceptor interactions between doubly occupied lone pair orbitals and unoccupied antibond orbitals. The results allow many of the quantitative trends in cluster structure, and spectroscopic properties to be rationalized in terms of non-pairwise-additive charge transfer delocalization between monomers.

## Acknowledgements

Financial support provided by the Deutsche Forschungsgemeinschaft and the Fonds der Chemischen Industrie is gratefully acknowledged. M.M. is grateful to Prof. Dr. K. Jurkschat (Universität Dortmund) for generous support.

[1] a) F. Vögtle, *Supramolecular Chemistry*, Wiley, Chichester, **1991**; b) J.-M. Lehn, *Supramolecular Chemistry: Concepts and Perspectives*, VCH, New York, **1995**; c) J.-M. Lehn, *Comprehensive Supramolecular Chemistry*, Pergamon, New York, **1996**; d) B. J. Holliday, C. A. Mirkin, *Angew. Chem.* **2001**, *113*, 2076; *Angew. Chem. Int. Ed.* **2001**, *40*, 2022; e) B. Moulton, M. J. Zaworotko, *Chem. Rev.* **2001**, *101*, 1629.

[2] a) L. Pauling, *Nature of the Chemical bond*, 3rd ed., Cornell University Press, New York, **1960**; b) G. A. Jeffrey, *An Introduction to Hydrogen Bonding*, Oxford University Press, Oxford, **1997**; c) G. R. Desiraju, T. Steiner, *The Weak Hydrogen Bond in Structural Chemistry and Biology*, Oxford University Press, Oxford, **1999**; d) C. B. Aakeröy, A. M. Beatty, *Aust. J. Chem.* **2001**, *54*, 409; e) R. Ludwig, *Angew. Chem.* **2001**, *113*, 1856; *Angew. Chem. Int. Ed.* **2001**, *40*, 1808; f) G. R. Desiraju, *Acc. Chem. Res.* **2002**, *35*, 565; g) L. J. Prins, D. N. Reinhoudt, P. Timmermann, *Angew. Chem.* **2001**, *113*, 2446; *Angew. Chem. Int. Ed.* **2001**, *40*, 2382.

[3] T. Steiner, *Angew. Chem.* **2002**, *114*, 50; *Angew. Chem. Int. Ed.* **2002**, *41*, 48.

[4] C. V. K. Sharma, A. Clearfield, *J. Am. Chem. Soc.* **2000**, *122*, 4394.

[5] a) P. Macchi, B. B. Iversen, A. Sironi, B. C. Chakoumakos, F. K. Larsen, *Angew. Chem.* **2000**, *112*, 2831; *Angew. Chem. Int. Ed.* **2000**, *39*, 2719; b) D. Braga, F. Grepioni, J. J. Novoa, *Chem. Commun.* **1998**, 1959; c) J. J. Novoa, I. Nobeli, F. Grepioni, D. Braga, *New. J. Chem.* **2000**, *24*, 5.

[6] a) M. E. Druyan, A. H. Reis, Jr., E. Gebert, S. W. Peterson, G. W. Mason, D. F. Peppard, *J. Am. Chem. Soc.* **1976**, *98*, 4801; b) A. H. Reis, Jr., S. W. Peterson, M. E. Druyan, E. Gebert, G. W. Mason, D. F. Peppard, *Inorg. Chem.* **1976**, *15*, 2748; c) E. Urnezius, J. D. Protasiewicz, *Main Group. Chem.* **1996**, *1*, 369; d) B. Twamley, C.-S. Hwang, N. J. Hardman, P. P. Power, *J. Organomet. Chem.* **2000**, *609*, 152.

[7] a) D. Fenske, R. Mattes, J. Löns, K. F. Tebbe, *Chem. Ber.* **1973**, *106*, 1139; b) N. K. Skvortsov, S. V. Toldov, V. K. Bel'skii, *Russ. J. Gen. Chem.* **1994**, *64*, 550; c) L. A. Aslanov, S. S. Sotman, V. B. Rybakov, L. G. Elepina, E. E. Nifant'ev, *Zh. Strukt. Khim.* **1979**, *20*, 758.

[8] a) V. A. Uchtman, R. A. Gloss, *J. Phys. Chem.* **1972**, *76*, 1298; b) G. Ohms, K. Krüger, A. Rabis, V. Kaiser, *Phosphorus, Sulfur Silicon Relat. Elem.* **1996**, *114*, 75; c) K. J. Langley, P. J. Squattrito, F. Adani, E. Montoneri, *Inorg. Chim. Acta* **1996**, *253*, 77; d) T. J. R. Weakley, *Acta Crystallogr.* **1976**, *B32*, 2889; e) V. V. Tkachev, L. O. Atovmyan, B. V. Timikhin, O. A. Bragina, G. V. Ratovskii, L. M. Sergienko, *Zh. Strukt. Khim.* **1986**, *27*, 121; f) R. K. Chadha, G. Ösapay, *Acta Crystallogr.* **1995**, *C51*, 2340.

[9] a) D. DeLaMatter, J. J. McCullough, C. Calvo, *J. Phys. Chem.* **1973**, *77*, 1146; b) S. W. Peterson, E. Gebert, A. H. Reis, Jr., M. E. Druyan, G. W. Mason, D. F. Peppard, *J. Phys. Chem.* **1977**, *81*, 466; c) E. Gebert, A. H. Reis, Jr., M. E. Druyan, S. W. Peterson, G. W. Mason, D. F. Peppard, *J. Phys. Chem.* **1977**, *81*, 471.

[10] K. Merz, A. Knüfer, *Acta Crystallogr.* **2002**, *C58*, o187.

[11] a) G. Ferguson, C. Glidewell, R. M. Gregson, P. R. Meehan, *Acta Crystallogr.* **1998**, *B54*, 129; b) P. S. Wheatley, A. J. Lough, G. Ferguson, C. J. Burchell, C. Glidewell, *Acta Crystallogr.* **2001**, *B57*, 95; c) C. Glidewell, G. Ferguson, A. J. Lough, *Acta Crystallogr.* **2000**, *C56*, 855; d) C. V. K. Sharma, A. J. Hessheimer, A. Clearfield, *Polyhedron* **2001**, *20*, 2095; e) A. H. Mahmoudkhani, V. Langer, *J. Mol. Struct.* **2002**, *609*, 97; f) A. H. Mahmoudkhani, V. Langer, *J. Mol. Struct.* **2002**, *609*, 55.

[12] A. H. Mahmoudkhani, V. Langer, *Cryst. Growth Des.* **2002**, *2*, 21.

[13] H. Guo, M. Karplus, *J. Phys. Chem.* **1994**, *98*, 7104.

[14] M. W. Wong, *Chem. Phys. Lett.* **1996**, *256*, 391.

[15] Selected geometrical data for $\mathbf{C_1}$, $\mathbf{C_2}$, and $\mathbf{P_2}$ calculated at the 1) B3LYP/6-31G*, 2) B3LYP/6-31+G*, and 3) B3LYP/6-311+G* level of theory are given in the Supporting Information.

[16] The average binding energies per molecule (per hydrogen bond) in each cluster were obtained as follows. First, the total energy of an optimized structure was corrected for the basis set superposition error (BSSE). The resulting CP-corrected total energy of each cluster was then divided by the number of molecules (of hydrogen bonds) within the cluster. The average energy per molecule (per hydrogen bond) thus obtained minus the calculated energy of the isolated monomer finally yields the binding energy per molecule $\Delta E_{bin}$ (per hydrogen bond $\Delta E^*_{bin}$).

[17] L. González, O. Mó, M. Yánez, J. Elguero, *J. Chem. Phys.* **1998**, *109*, 2685.

[18] a) G. Baum, E. C. Constable, D. Fenske, C. E. Housecroft, T. Kulke, *Chem. Commun.* **1998**, 2659; b) M. G. Barandika, M. L. Hernández-Pino, M. K. Urtiaga, R. Cortés, L. Lezama, M. I. Arriortua, T. Rojo, *J. Chem. Soc. Dalton Trans.* **2000**, 1469; c) A. J. Blake, N. R. Champness, P. A. Cooke, J. E. B. Nicolson, *Chem. Commun.* **2000**, 665; d) M. Mehring, G. Gabriele, S. Hadjikakou, M. Schürmann, D. Dakternieks, K. Jurkschat, *Chem. Commun.* **2002**, 834; e) H.-P. Wu, C. Janiak, G. Rheinwald, H. Lang, *J. Chem. Soc. Dalton Trans.* **1999**, 183; f) C. Janiak, S. Temizdemir, S. Dechert, W. Deck, F. Girgsdies, J. Heinze, M. J. Kolm, T. G. Scharmann, O. M. Zipffel, *Eur. J. Inorg. Chem.* **2000**, 1229.

[19] F. Weinhold, *J. Mol. Struct.* **1997**, *399*, 181.

[20] P. Gilli, V. Ferretti, V. Bertolasi, G. Filli, *Adv. Mol. Struct. Res.* **1996**, *2*, 67.

[21] C. A. Schalley, *Int. J. Mass Spect.* **2000**, *194*, 11.

[22] a) K. C. Russel, E. Leize, A. van Dorsselaer, J.-M. Lehn, *Angew. Chem.* **1995**, *107*, 244; *Angew. Chem. Int. Ed. Engl.* **1995**, *34*, 209; b) C. M. Drain, R. Fischer, E. G. Nolen, J.-M. Lehn, *J. Chem. Soc. Chem. Commun.* **1993**, 243; c) X. Cheng, Q. Gao, R. D. Smith, E. E. Simanek, M. Mammen, G. M. Whitesides, *J. Org. Chem.* **1996**, *61*, 2204.

[23] a) J. L. Sessler, R. Wang, *Angew. Chem.* **1998**, *110*, 1818; *Angew. Chem. Int. Ed.* **1998**, *37*, 1726; b) J. L. Sessler, R. Wang, *J. Org. Chem.* **1998**, *63*, 4079.

[24] a) P. Timmerman, K. A. Jolliffe, M. C. Calama, J.-L. Weidmann, L. J. Prins, F. Cardullo, B. H. M. Snellink-Ruel, R. H. Fokkens, N. M. M. Nibbering, S. Shinkai, D. N. Reinhoudt, *Chem. Eur. J.* **2000**, *6*, 4104; b) P. Timmerman, R. H. Vreekamp, R. Hulst, W. Verboom, D. N. Reinhoudt, K. Rissanen, K. A. Udachin, J. Ripmeester, *Chem. Eur. J.* **1997**, *3*, 1823; c) K. A. Jolliffe, M. C. Calama, R. Fokkens, N. M. M. Nibbering, P. Timmerman, D. N. Reinhoudt, *Angew. Chem.* **1998**, *110*, 1294; *Angew. Chem. Int. Ed.* **1998**, *37*, 1247; d) M. C. Calama, R. Hulst, R. Fokkens, N. M. M. Nibbering, P. Timmerman, D. N. Reinhoudt, *Chem. Commun.* **1998**, 1021.

[25] a) P. Bussian, F. Sobott, B. Brutschy, W. Schrader, F. Schüth, *Angew. Chem.* **2000**, *112*, 4065; *Angew. Chem. Int. Ed.* **2000**, *39*, 3901; b) W. Henderson, C. Evans, *Inorg. Chim. Acta* **1999**, *294*, 183.

[26] R. B. Cole, *Electrospray Ionization Mass Spectrometry*, Wiley, New York, **1997**.

[27] GAUSSIAN 98, Revision A.9, M. J. Frisch, G. W. Trucks, H. B. Schlegel, G. E. Scuseria, M. A. Robb, J. R. Cheeseman, V. G. Zakrzewski, J. A. Montgomery, R. E. Stratmann, J. C. Burant, S. Dapprich, J. M. Millam, A. D. Daniels, K. N. Kudin, M. C. Strain, O. Farkas, J. Tomasi, V. Barone, M. Cossi, R. Cammi, B. Mennucci, C. Pomelli, C.

  0947-6539/03/0904-0848 $ 20.00+.50/0 

Adamo, S. Clifford, J. Ochterski, G. A. Petersson, P. Y. Ayala, Q. Cui, K. Morokuma, D. K. Malick, A. D. Rabuck, K. Raghavachari, J. B. Foresman, J. Cioslowski, J. V. Ortiz, B. B. Stefanov, G. Liu, A. Liashenko, P. Piskorz, I. Komaromi, R. Gomperts, R. L. Martin, D. J. Fox, T. Keith, M. A. Al-Laham, C. Y. Peng, A. Nanayakkara, C. Gonzalez, M. Challachombe, P. M. W. Gill, B. G. Johnson, W. Chen, M. W. Wong, J. L. Andres, M. Head-Gordon, E. S. Replogle, J. A. Pople, Gaussian, Inc., Pittsburgh, **1998**.

[28] S. F. Boys, F. Bernardi, *Molec. Phys.* **1970**, *19*, 553.

[29] a) A. E. Reed, A. E. Curtiss, F. Weinhold, *Chem. Rev.* **1988**, *88*, 899; b) B. F. King, F. Weinhold, *J. Chem. Phys.* **1995**, *103*, 333; c) NBO 4.0 Program Manual, University of Wisconsin Theoretical Chemistry Institute Technical Report WISC-TCI-756 (USA: University of Wisconsin).

Received: August 20, 2002 [F4353]

  0947-6539/03/0904-0849 $ 20.00+.50/0 